PHILOSOPHICAL TRANSACTIONS OF THE ROYAL SOCIETY A MATHEMATICAL, PHYSICAL & ENGINEERING SCIENCES

A 40-million-year history of atmospheric CO_2

Yi Ge Zhang, Mark Pagani, Zhonghui Liu, Steven M. Bohaty and Robert DeConto

Phil. Trans. R. Soc. A 2013 **371**, 20130096, published 16 September 2013

PHILOSOPHICAL TRANSACTIONS OF THE ROYAL SOCIETY A

rsta.royalsocietypublishing.org

Research

Cite this article: Zhang YG, Pagani M, Liu Z, Bohaty SM, DeConto R. 2013 A 40-million-year history of atmospheric CO_2. Phil Trans R Soc A 371: 20130096.
http://dx.doi.org/10.1098/rsta.2013.0096

One contribution of 11 to a Discussion Meeting Issue 'Warm climates of the past—a lesson for the future?'.

Subject Areas:
climatology, geochemistry, oceanography

Keywords:
Cenozoic carbon dioxide, alkenone–pCO_2 method, carbon isotopes, benthic oxygen isotopes, global temperature, cryosphere

Author for correspondence:
Yi Ge Zhang
e-mail: yige.zhang@yale.edu

Electronic supplementary material is available at http://dx.doi.org/10.1098/rsta.2013.0096 or via http://rsta.royalsocietypublishing.org.

Royal Society Publishing
Informing the science of the future

A 40-million-year history of atmospheric CO_2

Yi Ge Zhang[1], Mark Pagani[1], Zhonghui Liu[2], Steven M. Bohaty[3] and Robert DeConto[4]

[1]Department of Geology and Geophysics, Yale University, New Haven, CT 06520-8109, USA
[2]Department of Earth Sciences, The University of Hong Kong, Hong Kong, People's Republic of China
[3]School of Ocean and Earth Science, National Oceanography Centre, University of Southampton, Southampton SO14 3ZH, UK
[4]Department of Geosciences, University of Massachusetts-Amherst, Amherst, MA 01003, USA

The alkenone–pCO_2 methodology has been used to reconstruct the partial pressure of ancient atmospheric carbon dioxide (pCO_2) for the past 45 million years of Earth's history (Middle Eocene to Pleistocene epochs). The present long-term CO_2 record is a composite of data from multiple ocean localities that express a wide range of oceanographic and algal growth conditions that potentially bias CO_2 results. In this study, we present a pCO_2 record spanning the past 40 million years from a single marine locality, Ocean Drilling Program Site 925 located in the western equatorial Atlantic Ocean. The trends and absolute values of our new CO_2 record site are broadly consistent with previously published multi-site alkenone–CO_2 results. However, new pCO_2 estimates for the Middle Miocene are notably higher than published records, with average pCO_2 concentrations in the range of 400–500 ppm. Our results are generally consistent with recent pCO_2 estimates based on boron isotope-pH data and stomatal index records, and suggest that CO_2 levels were highest during a period of global warmth associated with the Middle Miocene Climatic Optimum (17–14 million years ago, Ma), followed by a decline in CO_2 during the Middle Miocene Climate Transition (approx. 14 Ma). Several relationships remain contrary to expectations. For example, benthic foraminiferal $\delta^{18}O$ records suggest a period of deglaciation and/or high-latitude warming during the latest Oligocene (27–23 Ma) that, based on our results, occurred concurrently with a long-term

decrease in CO_2 levels. Additionally, a large positive $\delta^{18}O$ excursion near the Oligocene–Miocene boundary (the Mi-1 event, approx. 23 Ma), assumed to represent a period of glacial advance and retreat on Antarctica, is difficult to explain by our CO_2 record alone given what is known of Antarctic ice sheet history and the strong hysteresis of the East Antarctic Ice Sheet once it has grown to continental dimensions. We also demonstrate that in the Neogene with low CO_2 levels, algal carbon concentrating mechanisms and spontaneous biocarbonate–CO_2 conversions are likely to play a more important role in algal carbon fixation, which provides a potential bias to the alkenone–pCO_2 method.

1. Introduction

Knowledge of the partial pressure of atmospheric CO_2 (pCO_2), beyond direct measurements of atmospheric [1] and ice-core gas compositions over the last 800 000 years [2–4], derives from a range of techniques including stomatal indices of fossil leaves (e.g. [5–9]), the carbon isotopic compositions of palaeosol carbonate nodules (e.g. [10–12]), the boron isotopic compositions of shallow-dwelling foraminifera (e.g. [13–17]) and the stable carbon isotope compositions of algal biomarkers, such as alkenones (e.g. [18–24]). Most Cenozoic CO_2 reconstructions indicate substantially higher CO_2 values in the Early Eocene with a broad decrease during the Middle Eocene into the Neogene. However, a twofold variation in absolute pCO_2 concentrations persists among the available proxies during key climatic intervals [25].

Following the initial development of alkenone-based CO_2 reconstructions for the Pleistocene and Holocene [26,27], a revised methodology was applied for long-term CO_2 reconstructions for the Middle Eocene to the Pleistocene [18–20,22,23,28]. More than 20 marine localities have been used for Cenozoic reconstructions. However, the published Cenozoic alkenone–CO_2 record represents a stacked record from various ocean localities (e.g. [28]). This potentially introduces bias into CO_2 trends and magnitudes because temperature, nutrient conditions, seasonality and thermocline depth can impact algal growth conditions and contribute to variability in reconstructed CO_2 estimates. Thus, temporal CO_2 patterns from composite records could have trends specific to individual sites and not representative of changes in long-term global atmospheric conditions [21].

In this study, we present a continuous alkenone-based CO_2 record from one marine site for the past 40 million years to limit variability introduced by composite results. With this new record, we attempt to reconcile the discrepancy of CO_2-level reconstructions between alkenone and other proxies and explore CO_2 forcing in the context of global climate change since the late Middle Eocene. Also discussed is a preliminary assessment of the potential bias related to algal carbon concentrating mechanisms (CCMs) and spontaneous bicarbonate–CO_2 conversion, when using the alkenone–pCO_2 method to estimate the CO_2 levels in the Cenozoic.

2. Background

(a) The alkenone–pCO_2 method

(i) Diffusion versus active carbon uptake models of carbon transport

Alkenones occur as a suite of long-chained (C_{37}–C_{39}) unsaturated ethyl and methyl ketones produced by a few haptophyte algae in the modern ocean [29,30]. Today, the predominant sources of alkenones derive from *Emiliania huxleyi* (originating in the Late Pleistocene [31]) and *Gephyrocapsa oceanica* (originating in the Pliocene [32]). Sedimentary alkenones that pre-date the Pliocene were probably produced by haptophytes related to the family Noelaerhabdaceae and genera *Reticulofenestra* and *Dictyococcites* [33–37].

Alkenone-based pCO_2 reconstructions require paired measurements on stable carbon isotope composition of the di-unsaturated C_{37} methyl ketone ($\delta^{13}C_{37:2}$) and carbonates. Differences between the $\delta^{13}C$ of algal carbon and carbonate represent the total carbon isotope fractionation (ε_p) that occurs during algal growth. ε_p derived from $\delta^{13}C_{37:2}$ values ($\varepsilon_{p37:2}$) is calculated by the following equation:

$$\varepsilon_{p37:2} = \left[\frac{\delta_{CO_{2(aq)}} + 1000}{\delta_{org} + 1000} - 1\right] \times 1000, \tag{2.1}$$

where δ_{org} is the carbon isotopic composition of the algal cell estimated from the $\delta^{13}C$ of alkenone ($\delta_{37:2}$). The isotopic difference between δ_{org} and $\delta_{37:2}$ is 4.2‰, following earlier studies [26,27,38]:

$$\delta_{org} = \left[(\delta_{37:2} + 1000) \times \left(\left(\frac{4.2}{1000}\right) + 1\right)\right] - 1000, \tag{2.2}$$

where $\delta_{CO_{2(aq)}}$ is the $\delta^{13}C$ value of dissolved $CO_{2(aq)}$ approximated from the $\delta^{13}C$ values of shallow-dwelling foraminifera assuming isotopic and chemical equilibria among all inorganic carbon species, atmospheric CO_2 and foraminifera calcite tests (e.g. [26]).

The alkenone–CO_2 method is based on the assumption that the transport of inorganic carbon (dissolved CO_2) across the cell membrane to the site of carbon fixation within the algal cell predominantly occurs by diffusion. For diffusion transport, the total stable carbon isotope fractionation, which occurs during marine photosynthesis, is described by the following equation [39,40]:

$$\varepsilon_p = \varepsilon_t + (\varepsilon_f - \varepsilon_t)\left(\frac{C_i}{C_e}\right), \tag{2.3}$$

where C_e represents the ambient concentration of $CO_{2(aq)}$ ($[CO_{2(aq)}]$), C_i is the intracellular $[CO_{2(aq)}]$, ε_f is the total carbon isotope fractionation that occurs during photosynthesis and ε_t is the carbon isotope fractionation associated with carbon transport. Most alkenone-based pCO_2 reconstructions have adopted a range of ε_f values from 25 to 28‰ (e.g. [18–20,22–24]), consistent with the majority of algal growth experiments [41,42].

Chemostat incubations for two strains of alkenone-producing haptophyte algae and two diatoms, under continuous light- and nitrate-limited conditions show that ε_p linearly varies with $[CO_{2(aq)}]$, specific growth rate (μ) and cell geometry [42–44], consistent with a predominantly diffusion carbon transport model. By contrast, dilute batch cultures of *E. huxleyi* grown under nutrient-replete conditions and variable irradiance yield lower $\varepsilon_{p37:2}$ values, minor response to $[CO_{2(aq)}]$ changes [45] and an irradiance effect on the magnitude of $\varepsilon_{p37:2}$ [46]. Such results suggest that assumptions of a strictly diffusion carbon uptake model may not be valid under some nutrient and light conditions. For example, low $[CO_{2(aq)}]$ chemostat experiments for diatom *Phaeodactylum tricornutum* resulted in a nonlinear response of ε_p to $\mu/[CO_{2(aq)}]$, indicating that a CCM was triggered when the supply of $CO_{2(aq)}$ became limiting to growth (in this case, approx. less than 7 $\mu mol\, kg^{-1}$ [44,47]). CCMs are known to be available to a broad range of algal species [48–51]. However, whether or not ancient alkenone-producing algae were characterized by CCMs is presently unknown.

(ii) Simplified model of diffusion carbon uptake and palaeoclimate reconstructions

Various physiological factors have been shown to impact C_i (equation (2.3)) [52]. However, because C_i is difficult to constrain, Jasper & Hayes [26] recast equation (2.3) as

$$\varepsilon_p = \varepsilon_f - \frac{b}{[CO_2]}, \tag{2.4}$$

where the term b represents a range of physiological variables that encompass the combined effects of growth rate, cell geometry and other potential factors.

Surface water analysis of $\delta^{13}C_{37:2}$ and seawater chemistry show a strong relationship between b in equation (2.4) and the concentration of soluble phosphate [21,53]. Dissolved reactive phosphate ($[PO_4^{3-}]$) is a key macronutrient that often covaries with other biolimiting trace-metal

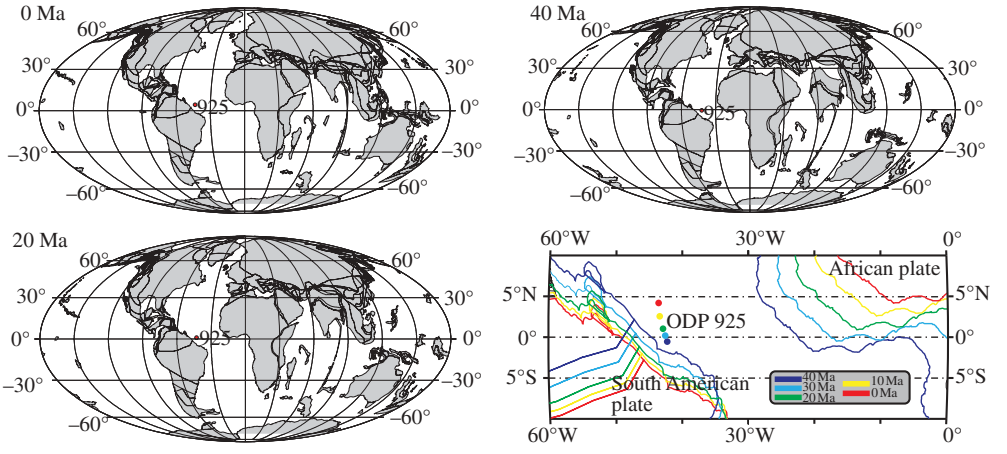

Figure 1. Global plate reconstruction shows the location of ODP Site 925 at 40, 20 Ma and the present, as well as a detail of the northward movement of Site 925 since 40 Ma [54]. Continents are shown as tectonic terrains rather than shorelines.

micro-nutrients, such as iron, zinc and cobalt [53], providing a link between $[PO_4^{3-}]$, growth rate and the value of ε_p.

Calibration of b with respect to $[PO_4^{3-}]$ using all available data (see [21]) results in the following relationships assuming $\varepsilon_f = 25‰$:

$$b = (118.52 \times [PO_4^{3-}]) + 84.07. \tag{2.5}$$

(iii) Uncertainties in pCO_2 calculations

If carbon assimilation is primarily determined by diffusion transport, ε_p is well described by equation (2.3). However, various other parameters, in addition to $CO_{2(aq)}$, are known to play a role in the expression of ε_p. Some of these parameters influence ε_p through a direct impact on C_i, including growth rate, irradiance, cell membrane permeability and cell size. CO_2 estimates are further compromised by uncertainties in phosphate concentrations used to estimate the physiological-dependent term b, as well as the potential of regionally different b versus $[PO_4^{3-}]$ relationships relative to the global calibration. Assumptions regarding the value of enzymatic isotope fractionation (ε_f), as well as knowledge of sea surface temperatures (SSTs)—generally obtained from various geochemical proxies—further contribute to CO_2 uncertainties [21]. Finally, other factors, such as CCMs, probably arise when the intracellular concentration of CO_2 becomes limiting. CCMs can impact the value of ε_p by transporting different carbon species with specific carbon isotopic compositions, and altering C_i relative to diffusive flux. Also, isotope fractionations associated with active transport mechanisms are likely distinct.

(b) Site location

Ocean Drilling Program (ODP) Site 925 (4°12.25′N, 43°29.33′W, 3042 m water depth) is located on Ceara Rise in the western equatorial Atlantic Ocean (figure 1) [55]. Modern surface waters at this site are characterized by high mean annual SST (approx. 27.5°C) and low nutrient levels (surface $[PO_4^{3-}]$ approx. 0.14 µmol l^{-1} [56]). The Middle Eocene to Pleistocene sedimentary succession recovered at Site 925 consists of pelagic carbonate oozes and chalks, primarily foraminifer-bearing nannofossil oozes with minor amounts of clay. All samples used in this study were taken from ODP Hole 925A. Previously reported Plio-Pleistocene pCO_2 data are based on Hole 925C and 925D [22].

Palaeogeographic reconstructions indicate that this site has moved northward over the past 40 Ma, from just south of the equator during the Late Eocene, to approximately 4°N today

(figure 1) [54]. Site 925 was right on the equator around 30 Ma. Available mass accumulation rates of biogenic barium and reactive phosphorus suggest stable productivity and nutrient conditions from 36.9 to 32.7 Ma [57]. Calcareous nannofossils indicate weak to moderate tropical upwelling history [55] consistent with a minor air–sea CO_2 disequilibrium expressed today, with modern surface waters enriched by approximately 22 ppm [58].

3. Material and methods

(a) Lipid extraction and analysis

Approximately 40–100 g of sediment (dry weight) were used for biomarker analysis. Samples were freeze-dried and extracted with dichloromethane/methanol (2 : 1, v/v) using an Accelerated Solvent Extractor (ASE 300, Dionex) at 120°C and 10.3 MPa. Total lipid extracts (TLEs) were concentrated under a stream of purified N_2 using a Zymark Turbovap II, and then separated into three fractions using silica gel chromatography. TLEs were separated into compound classes using ashed Pasteur pipettes loaded with approximately 4 g deactivated silica gel (70–230 mesh), and sequentially eluted with 2 ml hexane, 4 ml dichloromethane and 4 ml methanol to obtain aliphatic, aromatic and polar fractions, respectively.

The dichloromethane fraction containing ketones was subject to basic hydrolysis and silver nitrate column chromatography to purify long-chain alkenones. Relative abundances of di- and tri-unsaturated methyl ketones were analysed on a Thermo Trace 2000GC equipped with an Rxi-1 ms column (60 m × 0.25 mm × 0.25 µm), a programmed temperature vaporization (PTV) injector and a flame ionization detector with He as the carrier gas. The oven was set to 90°C upon sample injection, held for 1 min, ramped up at 20°C min^{-1} to 280°C, then 2°C min^{-1} to 320°C. Temperature was held constant at 320°C for 30 min. The relative abundance of C37 : 2 and C37 : 3 alkenones was used to compute $U^{k'}_{37}$, a proxy developed to reconstruct ancient SSTs [59,60]. Analytical precision, determined through multiple analyses of an in-house alkenone standard, represents an uncertainty of ±0.005 $U^{k'}_{37}$ units (see electronic supplementary material).

The methanol fraction containing glycerol dialkyl glycerol tetraethers (GDGTs) was further purified by passing through activated alumina dissolved in dichloromethane/methanol (1 : 1, v/v). The eluting fraction was dried under pure N_2 stream, then dissolved in an azeotrope of hexane/isopropanol (99 : 1, v/v) and filtered through an ashed 0.7 µm glass microfibre filter. Analyses of GDGTs were conducted following a slightly modified method described by Hopmans *et al*. [61]. Compound identification and relative abundance analyses were determined using an Agilent 1200 high-performance liquid chromatography/atmospheric pressure chemical ionization mass spectrometer (HPLC/APCI-MS). Separation of GDGTs was achieved on an Alltech Prevail cyano column (150 mm, 2.1 mm I.D., and 3 µm grain size) kept at 30°C. The following solvent polarity gradient was used, based on A: hexane/isopropanol (99 : 1, v/v), and B: hexane/isopropanol (90 : 10, v/v): 100% solvent A for 5 min, then solvent B was linearly increased from 0% at 5 min, to 7.4% at 40 min, and maintained from 40 to 50 min. After each sample analysis, the column was back flushed with 100% solvent B for 14 min, followed by 10 min equilibration with normal phase flow of 100% solvent A. Mass spectrometric identification and quantification were achieved using an Agilent 6130 ion-trap mass spectrometer coupled to the HPLC by an APCI interface. Ion scans were set to m/z 1200–1500. Quantification was based on peak intensities in the mass chromatogram of the $[M + H]^+$ ions. Relative abundance of GDGTs was used to calculate TEX_{86}, a proxy employed to estimate past SSTs [62]. Repeated measurements of an in-house laboratory standard showed the analytical precision represented ±0.01 TEX_{86} units (see electronic supplementary material).

(b) Carbon isotope measurements

Carbon isotopic compositions of $C_{37:2}$ alkenones were analysed on a Thermo Finnigan MAT 253 mass spectrometer interfaced with a Trace GC Combustion III (GC-IRMS) equipped with

a PTV injector and a J&W Scientific DB-1 capillary column (60 m × 0.25 mm × 0.25 mm), using He as a carrier gas with a flow speed of 2.0 ml min^{-1}. GC temperature was held at 60°C for 1 min, increased to 320°C at 15°C min^{-1} and held isothermally for 35 min. Carbon isotopes are reported relative to the VPDB standard based on an in-house reference gas calibrated to the OzTech standard ($\delta^{13}C = -40.61‰$). A C_{20} *n*-alkane standard was injected daily to determine the analytical accuracy of the carbon isotope measurements, yielding an uncertainty of ±0.2‰. $U^{k'}_{37}$ and $\delta^{13}C_{37:2}$ data reported for the Eocene–Oligocene climate transition [21] and the Pliocene–Pleistocene [22] have been previously published (see electronic supplementary material).

(c) Foraminifera stable isotope measurements

Splits of samples were wet sieved with deionized water at 63 µm. Surface-dwelling planktic foraminifera, including *Globigerinoides ruber*, '*Globigerinoides ruber* s.1.' and *Globigerinoides altiaperturus*, were picked from the 250–300 µm sieve fraction in the Neogene section, and epifaunnal benthic foraminifera (*Cibicidoides* spp.) were picked from greater than 250 µm sieve fraction throughout the entire Site 925 study section. Carbon stable isotope analysis of the picked foraminiferal samples was performed using a Europa GEO 20–20 mass spectrometer at the University of Southampton. Samples were reacted with phosphoric acid at 70°C using an automatic carbonate preparation system 'CAPS' in line with the mass spectrometer. Typically, five to eight benthic specimens from each sample were combined and analysed together, and 15–20 planktic specimens were analysed together. All values are reported relative to the VPDB scale, with an external analytical precision estimated at 0.08‰ for $\delta^{13}C$ (see electronic supplementary material).

(d) Chronology

Age determinations for ODP Hole 925A are based on biostratigraphy planktic foraminifera [63,64] with 75 age control points based on first and last occurrence data (see electronic supplementary material) over a span of 40 million years. All data are calibrated to the geomagnetic polarity timescale of [65] and the integrated timescale of Berggren *et al*. [66].

4. Results

(a) Temperature

SSTs based on $U^{k'}_{37}$ and TEX_{86} indices were reconstructed for the past 40 Ma using the linear calibration of Conte *et al*. [67] and the reciprocal calibration of Liu *et al*. [68], respectively (figure 2*a*). $U^{k'}_{37}$ SST reconstructions indicate relatively constant temperatures of approximately 28°C since the Late Eocene, except for an approximately 2°C cooling during the Pliocene–Pleistocene interval. However, 28.5°C represents maximum temperatures expressed by the $U^{k'}_{37}$ calibration ($U^{k'}_{37}$ value reaches 1), and therefore warmer temperatures above approximately 28°C cannot be determined. By contrast, maximum temperatures associated with the TEX_{86} proxy are unconstrained. Reconstructed TEX_{86} records exhibit much larger fluctuations compared with $U^{k'}_{37}$ with temperatures of approximately 30°C in the Late Eocene that fall to approximately 22°C during the Late Pliocene—more than 5°C cooler at the same locality today. However, the TEX_{86}-based temperatures since Pliocene might suffer from additional GDGT inputs, as indicated by high BIT values (mean value is 0.6; electronic supplementary material) [69].

In order to estimate CO_2, we do not favour one SST proxy over the other for the entire 40 million year record from Site 925. Instead, we selected the highest temperature estimates from both $U^{k'}_{37}$ and TEX_{86} records to synthesize a composite temperature profile. Differences between $U^{k'}_{37}$ and TEX_{86} records are considered to reflect the uncertainty of SST reconstructions at each sample, which is further used in the computation of $\varepsilon_{p37:2}$ and pCO_2. We also realize that different

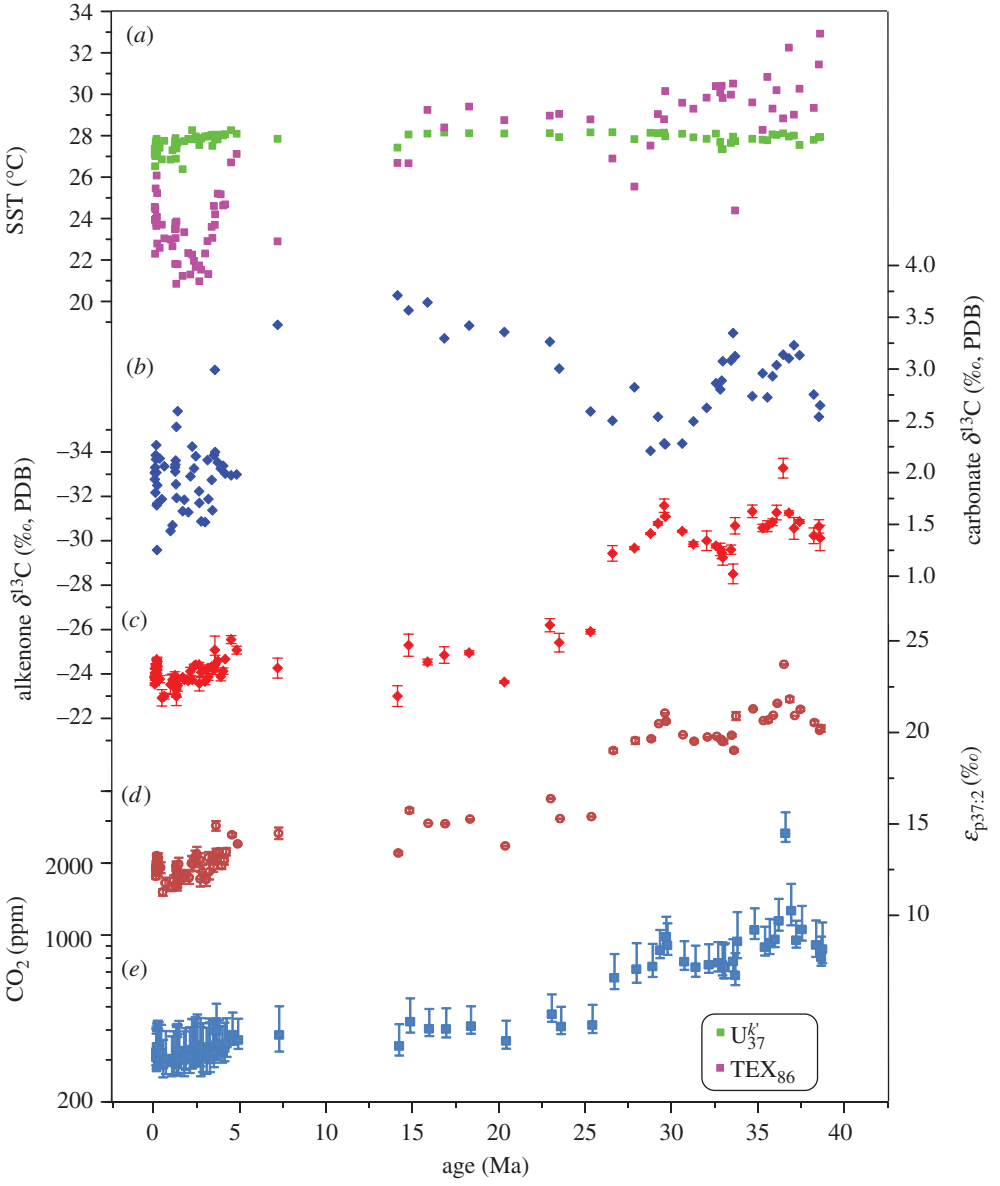

Figure 2. Time series of ODP Site 925. (*a*) $U^{k'}_{37}$- and TEX_{86}-based SST reconstruction. (*b*) Adjusted carbon isotopes from foraminiferal stable isotope measurements to proximate $\delta^{13}C$ of surface water dissolved inorganic carbon. (*c*) Carbon isotopes of alkenones; (*d*) $\varepsilon_{p37:2}$ calculated from (*b*) and (*c*); (*e*) pCO_2 calculated from (*d*), using both $U^{k'}_{37}$- and TEX_{86}-based SST estimates, and assuming $[PO_4^{3-}]$ values were 0.20, 0.14 (lower limit) and 0.39 μM (upper limit). Refer to electronic supplementary material to see details of constructing (*b*,*d*,*e*) and their related uncertainties; one CO_2 estimate at 35.52 Ma gives a value more than 2400 ppm, which is off the chart and therefore not shown in the following figures.

calibrations for $U^{k'}_{37}$- and TEX_{86}-SST conversion could introduce additional uncertainties, but they are secondary compared with the difference between the two proxies themselves.

(b) Carbon isotopes and $\varepsilon_{p37:2}$

Planktonic foraminifera are partially to fully recrystallized in the Upper Eocene–Lower Oligocene interval of Site 925. $\delta^{13}C$ measurements on the presumed surface water dwellers *Turborotalia* spp.

show only small differences (0.1–0.5‰) from the benthic *Cibicidoides* spp. within the same sample, suggesting that *Turborotalia* either maintained a thermocline habitat or is affected by diagenetic alteration [21]. However, agreement between *Cibicidoides* $\delta^{13}C$ values at Site 925 and an Eocene–Oligocene Southern Ocean compilation of $\delta^{13}C$ values from ODP Sites 689, 733, 744 and 748 suggests adequate preservation of $\delta^{13}C$ values [21]. Consequently, Pagani *et al*. [21] reconstructed surface $\delta^{13}C$ by measuring *Cibicidoidis* $\delta^{13}C$ values, assuming a constant offset (0.94‰) between surface and deep waters $\delta^{13}C_{DIC}$.

Miocene mixed-layer foraminifera are better preserved than Palaeogene specimens. *Globogerinoides altiaperturus* were measured in the Early Miocene and *G. ruber* s.1. were selected in the Mid- to Late Miocene interval. A $\delta^{13}C$ offset of 0.94‰ with an ascribed uncertainty of ±0.3‰ [70] was applied to both *G. ruber* and *G. altiaperturus* $\delta^{13}C$ values to estimate surface water $\delta^{13}C_{DIC}$ (figure 2*b*). The planktic foraminifera approach in the Miocene is accompanied by benthic foraminifera *Cibicidoides* $\delta^{13}C$ analyses and the applications of assumed surface–deep water isotopic offsets. Results show that the two independent approaches are within 0.20‰ from each other (see electronic supplementary material). Carbon isotope compositions on the shallow-dwelling *Globogerinoides sacculifer* since 5 Ma have been previously reported (figure 2*b*) [22].

$\delta^{13}C_{37:2}$ values are more ^{13}C depleted during the Palaeogene relative to the Neogene (figure 2*c*). Calculation of $\delta^{13}C$ of surface seawater aqueous CO_2 is by converting the mixed-layer $\delta^{13}C_{DIC}$ (figure 2*b*), using the composite temperature estimates and associated uncertainties from organic geochemical proxies (§4*a*), assuming equilibrium isotopic fractionations between different carbonate species. Aqueous CO_2 $\delta^{13}C$ and $\delta^{13}C_{37:2}$ are further used to calculate $\varepsilon_{p37:2}$.

Figure 2 shows that variability in $\delta^{13}C_{37:2}$ is predominantly responsible for the character of $\varepsilon_{p37:2}$ trends. $\varepsilon_{p37:2}$ values exhibit a long-term decreasing trend, with the majority of $\varepsilon_{p37:2}$ varying between 21 and 18‰ during the Late Eocene to Early Oligocene, 16–13‰ in the Late Oligocene/Miocene and 13–11‰ during the Pliocene/Pleistocene (figure 2*d*).

(c) pCO_2 estimates

We assume a value of 25‰ for ε_f [41,42,44], and a range of $[PO_4^{3-}]$ from 0.14 to 0.39 µM, representing the present-day phosphate concentrations from 0 to 100 m near Site 925 [56], with 50 m (0.20 µM) to be the most representative depth for alkenone production. Estimates of pCO_2 were then calculated assuming air–sea equilibrium and proxy temperatures (the composite temperature, see §4*a*) using Henry's law (figure 2*e*). The uncertainty of pCO_2 is constrained by the variability of temperature and phosphate estimates. The maximum pCO_2 is calculated by using the upper limit of the ε_p, highest phosphate level and highest temperature estimates; whereas the minimum of pCO_2 is a result of the lower limit of ε_p, lowest phosphate and lowest temperature (see §4*a*,*b* for the determination of uncertainties associated with temperature and ε_p). The resulting uncertainty of pCO_2 estimates averages 38%, much larger than an error propagation model through Monte Carlo procedure (11%) with assumed uncertainty of different parameters used in pCO_2 calculations [20].

5. Discussion

(a) Comparisons between Site 925 and published Cenozoic pCO_2 records

Our new CO_2 results from Site 925 (figures 3 and 4) broadly agree with previously published composite alkenone–pCO_2 record for the Cenozoic [28]. Nevertheless, systematic differences are apparent with the new record indicating higher CO_2 levels after approximately 32 Ma (figure 3). This discrepancy can be explained, in part, by regional differences in oceanography and algal growth conditions, as expressed by variable ε_p values. For example, the Miocene average ε_p at

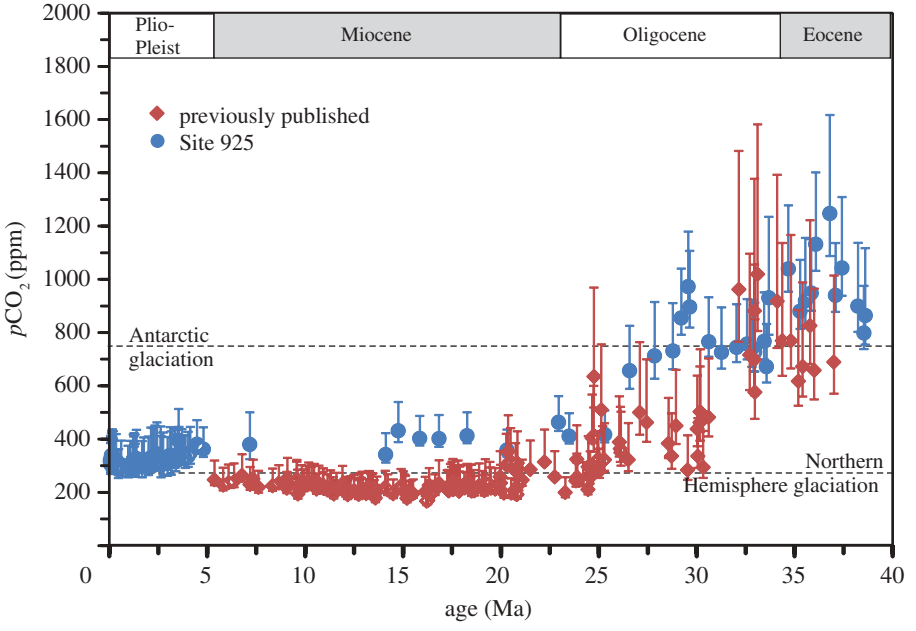

Figure 3. A comparison of alkenone-based pCO_2 composite from multiple marine sites as compiled in the study of Pagani *et al.* [28] and ODP Site 925 record since the Late Eocene. Antarctic glaciation thresholds (approx. 750 ppm) and Northern Hemisphere glaciation threshold (approx. 280 ppm) deduced from climate models [71] are marked by dashed lines.

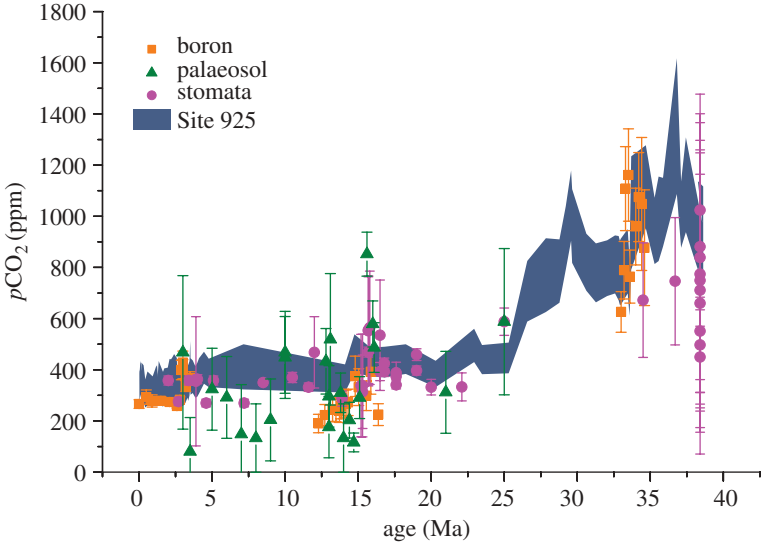

Figure 4. Comparison between different proxy-based pCO_2 estimates for the past 40 Ma. Boron isotope, palaeosol and stomata data are summarized by Beerling & Royer [25], with additional data from Foster *et al.* [15].

Site 925 is approximately 15‰, significantly higher than the mean value of approximately 10‰ at Deep Sea Drilling Project (DSDP) Site 588 [19,20]. Furthermore, new SST estimates (e.g. [19,20]) are used in this study, and these new $U^{k'}_{37}$- and TEX_{86}-based temperature records are considerably warmer during the Miocene to Early Pliocene, compared with foraminifer $\delta^{18}O$-based estimates (6–8°C, DSDP Site 588 [22]). Warmer SST estimates increase calculated pCO_2 levels [22].

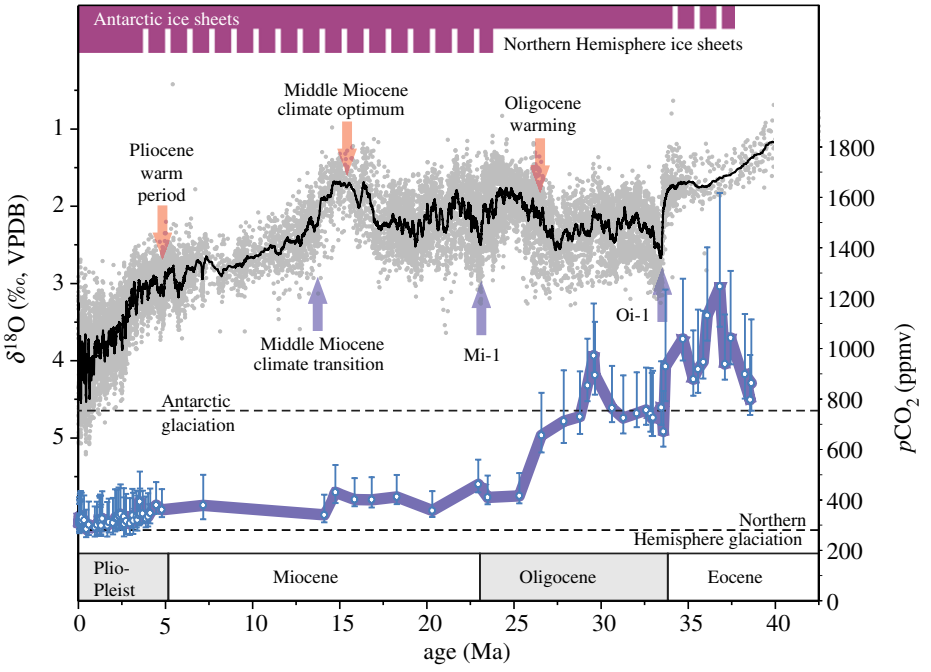

Figure 5. Climate and atmospheric CO_2 history for the past 40 Ma. Benthic $\delta^{18}O$ from Zachos *et al*. [72]. Major warming (red arrows) and cooling (blue arrows) events are labelled. Red bars indicate brief history of Antarctic and Northern Hemisphere ice sheets. Antarctic glaciation thresholds (approx. 750 ppm) and Northern Hemisphere glaciation threshold (approx. 280 ppm) deduced from climate models [71] are marked by dashed lines.

Finally, comparison of our new record with recent CO_2 reconstruction efforts, with putatively improved techniques and higher quality data [25], suggests broad agreement with boron isotope-pH [13,15,16], stomata [5–9] and palaeosol estimates [10–12], although palaeosol estimates have inherently larger uncertainties (figure 4).

(b) Palaeoclimate implications

(i) The late Middle Eocene to Early Oligocene

Coupled climate–ice sheet model simulations of the Eocene/Oligocene climate transition indicate that sudden nonlinear jumps in ice volume can be triggered by the congruence of favourable orbital cycles when pCO_2 concentrations decrease to 2.5–3 times pre-industrial levels (approx. 750 ppm; figure 5) [71,73]. Independent proxy reconstructions of pCO_2 across the Eocene–Oligocene transition, including those estimated by the boron isotope-pH methodology [16] and alkenone-based CO_2 records from Site 925 [21], support these model results and suggest CO_2 began to decrease immediately prior to the Oi-1 event and declined during the climate transition, probably falling below the approximately 750 ppm threshold.

Compared with a multi-site approach, oceanography and algal growth conditions might be less variable in a single site. However, the Late Eocene–Early Oligocene CO_2 record at Site 925 may still carry features that are specific to this locality. Although no major tropical upwelling has been detected throughout the entire record by calcareous nannofossil assemblages [55], plate reconstructions indicate that Site 925 tectonically moved from the Southern to the Northern Hemisphere and was positioned on the equator around 30 Ma (figure 1). This transit would have altered the expression of local sea surface CO_2, particularly at the equator where the convergence of trade winds drives upwelling of CO_2-rich deep waters [74]. A distinct

spike in ε_p values and reconstructed pCO_2 is evident in the Middle Oligocene (approx. 29.5 Ma, figure 2*d*), representing about 10–30% increase in CO_2 from the background level. The magnitude of present-day equatorial upwelling, however, is represented by a seawater CO_2 enrichment in the western equatorial Atlantic by approximately 30 ppm—about 9% deviation from atmosphere–seawater equilibrium [58]. This potentially implies that equatorial upwelling only partially contributed to the Middle Oligocene pCO_2 spike recorded in Site 925, or that upwelling intensity was higher and/or upper water-column stratification was less intense during the Oligocene.

(ii) The Late Oligocene to Early Miocene

Climatic behaviour during the Late Oligocene/Early Miocene interval is particularly difficult to explain given existing CO_2 records. After a period of gradual cooling following the onset of glaciation on Antarctica near the Eocene–Oligocene climate transition at approximately 34 Ma, an approximately 0.8‰ decrease in benthic $\delta^{18}O$ values (ODP 1218, eastern equatorial Pacific [75]) suggests a period of substantial warming and/or deglaciation during the latest Oligocene (approx. 27–23 Ma; figure 5). However, our corresponding CO_2 records indicate a long-term decrease in atmospheric carbon dioxide through the Late Oligocene (figure 5). Isotopic evidence for warming and/or partial deglaciation at the end of the Oligocene is not simply an artefact of stacked benthic $\delta^{18}O$ records from different marine sites [72,75] given that the $\delta^{18}O$ record from ODP Site 1218 spans the entire Oligocene and unambiguously supports the presence of a negative oxygen isotope excursion during this time [75]. Thus, the cause for this negative $\delta^{18}O$ trend remains unresolved in relation to our new CO_2 record.

Another apparent decoupling between CO_2 and climate occurs near the Oligocene–Miocene boundary (approx. 23 Ma), represented by a transient, positive benthic foraminiferal $\delta^{18}O$ excursion (greater than 1‰) interpreted as a period of substantial glaciation (known as the Mi-1 event) [76]. Our records suggest invariant CO_2 concentrations during this apparent glaciation/deglaciation, defying our current understanding of the necessary forcing required to drive Antarctic ice sheet variability.

Assuming approximately 2°C of cooling in the deep sea [77], approximately 0.5‰ of the 1‰ $\delta^{18}O$ shift at Mi-1 must have been driven by an increase in ice volume. If continental ice on Antarctica had an average isotopic composition of −40‰, as indicated by isotopic modelling [71], then more than 22×10^6 km^3 of ice—roughly equivalent to the entire present-day East Antarctic Ice Sheet (EAIS)—must have accumulated within 400 000 years. However, CO_2 levels during the Oligocene appear low enough to have already maintained a fully glaciated Antarctica according to ice sheet simulations [78]. Moreover, the recovery phase of Mi-1 is even more enigmatic because models require substantially higher CO_2 levels—at least two times higher than the formation threshold of the EAIS (approx. 1500 ppm) to cause substantial ice sheet retreat [71,78]. Coupled climate–ice sheet simulations show that orbital forcing alone cannot cause Antarctic deglaciation once the ice sheet expands over the continent [73], and requires increases in greenhouse gas concentrations to more than four times pre-industrial levels to cause substantial ice retreat [78]. It is possible that the resolution of our new CO_2 record is too low to resolve large fluctuations within the body of the Mi-1 event. Still, exiting the glacial period would require substantially higher CO_2 levels that are not detected in our record. Alternatively, polar climate sensitivity to CO_2 might have been much higher than simulated in climate models, or our understanding of Antarctic ice physics is incomplete and ice sheet stability, potentially reflected by the 'Oi' and 'Mi' events (e.g. [75]), is far more sensitive and dynamic than indicated in modelling studies. Another possibility is that the assumption that benthic $\delta^{18}O$ variability is representative of global temperature/ice volume is flawed. For example, Nd isotope records suggest alternating deep water sources during the Palaeogene [79,80], with the potential to alter the temperature, salinity and $\delta^{18}O$ value of deep waters. Different deep water sources during the Late Oligocene and the Mi-1 event could have played a role in the magnitude of the observed benthic $\delta^{18}O$ fluctuations.

Apparent discrepancies between proxy records of ice volume and CO_2 could also result if alkenone–CO_2 estimates are simply incorrect or biased for some time intervals. Various theoretical and empirical exercises have been performed to assess non-CO_2 factors that impact algal carbon isotope fractionation and uncertainties in alkenone–pCO_2 estimations [50,52]. For example, higher ambient CO_2 levels during the earlier part of the Cenozoic could have contributed to a reduction in bicarbonate uptake via β-carboxylation, resulting in ε_f values greater than 25‰ [21], as well as inhibiting CCMs. The isotopic impact of CCM upregulation during low CO_2 would arguably minimize ε_p and reconstructed CO_2 variability, which is discussed in greater detail in §5*c*.

(iii) The Mid- to Late Miocene

Very low Miocene pCO_2 concentrations that characterize published alkenone (figure 3) [19,20] and boron isotope [81] CO_2 records have puzzled the palaeoclimate community for nearly a decade. If atmospheric CO_2 was a key parameter forcing cryosphere expansion during the Neogene, then major Northern Hemisphere glaciation should have arguably occurred some 20 million years earlier than the accepted age of approximately 2.7 Ma (figure 3) [71,82,83]. Low pCO_2 levels are also difficult to reconcile with the well-documented warmth of the Middle and Late Miocene, which was characterized by SSTs significantly higher than today [84]. For example, subtropical east Pacific (ODP 1010) and northeast Pacific (ODP 1021) have been found to be at least 12°C warmer at 12 Ma relative to today, and 5°C warmer relative to the Early Pliocene [84]. Prior alkenone and boron isotope reconstructions have both indicated that the global warmth of the Middle Miocene climate optimum (MMCO, approx. 17–14 Ma) and the subsequent expansion and stabilization of Antarctic ice sheets (Middle Miocene climate transition (MMCT) approx. 14 Ma) were associated with relatively invariant pCO_2 [20,81] and slightly higher pCO_2 during ice expansion (figure 3) [20]. Not surprisingly, climate models applying published alkenone and boron isotope-based CO_2 records [85,86] cannot simulate Middle Miocene climate signals as determined by proxy records [19,81].

Intriguingly, our new record implicates a more important role for pCO_2 in the climatic variability of the Early to Middle Miocene. The partial pressure of carbon dioxide rises to 400–500 ppm during the climatic optimum of the Middle Miocene followed by an approximately 100 ppm decline during MMCT (figure 5), which better agrees with recent stomatal index [6] and boron isotope estimates (figure 4) [15]. Comparing the Site 925 record with the earlier alkenone–pCO_2 record from DSDP Site 588 [19,20], we found that the isotopic fractionation $\varepsilon_{p37:2}$ is larger (15‰ versus 10‰) and the SST estimate is higher by 6–8°C, both of which could have contributed to higher Miocene CO_2 levels in the new assessment. Although we cannot rule out the possibility that CO_2 air–sea disequilibrium at Site 925 contributed to higher local CO_2 estimates, three independent methods agree that pCO_2 during the MMCO was higher, and then declined during the MMCT cooling, implying that CO_2 was closely linked to major Miocene climate events. Importantly, Miocene CO_2 levels now appear higher than Pliocene and Pleistocene concentrations, consistent with the appearance of Northern Hemisphere glaciation during the Pliocene (figures 3 and 5).

(c) Assessing the effect of bicarbonate–CO_2 conversion

The capacity for active carbon transport is common among marine and fresh water algae [48,49,51]. This is because ribulose-1,5-bisphosphate carboxylase/oxygenase, the primary carboxylase, has a relatively low affinity for CO_2 and, for most algal species, is less than half saturated under current CO_2 levels [51]. CCMs increase carbon availability and reduce rates of photorespiration that impact rates of carbon fixation [51].

Whether or not CCMs were an important aspect of ancient alkenone producers remains speculative. Whereas some organisms, such as diatoms, show highly efficient and active CCMs [48,87], CCMs in modern *E. huxleyi* and other coccolithophores appear weakly expressed [53,88]. Physiological parameters of extinct alkenone-producing species are unknown. Since CCMs

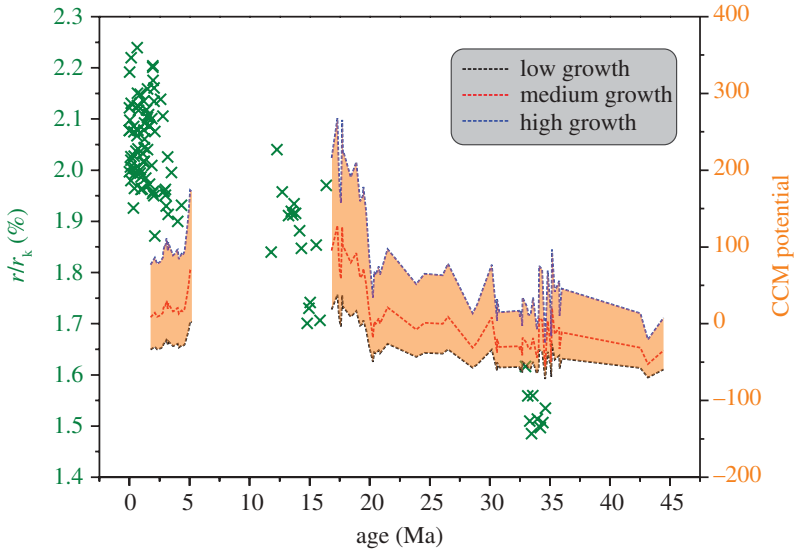

Figure 6. Comparison between the spontaneous bicarbonate–$CO_{2(aq)}$ conversion (green symbols) and the CCM potential of alkenone producers (orange bands) for the past 45 Ma. $HCO_3^- - CO_{2(aq)}$ conversion (r/r_k) based on the model of Riebesell *et al*. [90] and Wolf-Gladrow *et al*. [91], using seawater pH and SST data provided by boron isotope studies [13,15,16,18], and a constant radius of 2.67 μm for alkenone-producing haptophyte algae. Computation of CCM potential is based on the model of [44,50], using previously published cell size [21,37,89,92] and existing palaeo-CO_2 estimates [18,21,28]. CCM potential ($[(\mu/C_e)/(P/C)]100 - 100$) represents an arbitrary, qualitative scale of CCM activity.

are energetically expensive, ancient haptophytes probably lacked operational CCMs under the significantly higher CO_2 levels of the past [89]. However, the presence of CCMs could have become more pronounced during the Neogene due to the considerable decline in atmospheric CO_2 (figures 3–6). If this perspective is valid, then quantitative CO_2 reconstructions could be compromised during periods of relatively low pCO_2 levels.

Various theoretical models have been developed to understand the factors that would drive upregulation of CCMs [47,50,90,91]. One model assumes that active transport occurs when diffusive flux achieves a minimum threshold of intracellular CO_2 necessary for adequate growth. Minimum diffusive flux estimates depend on ambient $[CO_{2(aq)}]$ and constraints imposed by cell size. Assuming spherical geometry, minimum $[CO_{2(aq)}]$ can be defined as [47,90,91]

$$[CO_2]_{min} = \frac{F_{in}}{4\pi r D_T (1 + r/r_k)}, \tag{5.1}$$

where F_{in} is the diffusive influx of $CO_{2(aq)}$, D_T is the diffusion coefficient of CO_2, r is the 'surface area equivalent' spherical cell radius [91], r_k is the reacto-diffusive length (i.e. length of the boundary layer where HCO_3^- has the opportunity to convert to $CO_{2(aq)}$), and the term $(1 + r/r_k)$ represents the contribution of extracellular, uncatalysed and spontaneous $HCO_3^- - CO_2$ conversion to the total supply of CO_2 [47,90].

The term r_k is calculated by

$$r_k = \sqrt{\frac{D_T}{k'}} \tag{5.2}$$

where k' is the rate constant for conversion of HCO_3^- and H_2CO_3 to $CO_{2(aq)}$. An approximation for the temperature dependence of D_T is given by [93]

$$D_T = 5.019 \times 10^{-6} e^{-(E_d/RT_K)}, \tag{5.3}$$

with activation energy $E_d = 19\,510\,\mathrm{J\,mol^{-1}}$, gas constant $R = 8.3143\,\mathrm{J\,K^{-1}\,mol^{-1}}$ and T_K is temperature in kelvin. For the rate constant k', Gavis & Ferguson [94] demonstrated that

$$k' = k_1[\mathrm{OH^-}] + k_2, \tag{5.4}$$

where k_1 and k_2 are the rate constants of formation of CO_2 from HCO_3^- and H_2CO_3, respectively, and $[OH^-]$ is the hydroxyl ion concentration. At 25°C, $k_1 = 8500\,\mathrm{m^3\,mol^{-1}\,s^{-1}}$ and $k_2 = 3 \times 10^{-5}\,\mathrm{s^{-1}}$ [94].

Given the equilibrium constant for seawater $K_w = [H^+][OH^-]$, $[OH^-]$ can be calculated if seawater pH is known. At atmospheric pressure [95],

$$\ln K_w^* = 148.96502 - 13847 \times \frac{26}{T_K} - 23.6521 \ln T_K + \left[\frac{118.67}{T_K} - 5.977 + 1.0495 \ln T_K\right] S^{1/2} - 0.01615S. \tag{5.5}$$

Therefore, the portion of fixed CO_2 contributed by the conversion of bicarbonates in the geological past can be calculated if seawater temperature (T_K), pH, salinity (S) and the cell size (r) of ancient alkenone producers are constrained.

Ocean pH estimates and SST reconstructions are available for the Eocene–Oligocene climate transition [16], Middle Miocene [15], Pliocene [18] and the Pleistocene [13], and ancient cell sizes for assumed alkenone producers (e.g. *Reticulofenestra*, *Dictyococcites* and *Cyclicargolithus*) can be estimated using coccolith size measurements [21,37,89,92]. However, the available coccolith length data and boron-based pH estimates are not derived from the same marine sites. Cell sizes of assumed alkenone producers show large spatial variability. For example, Pagani *et al*. [21] demonstrated that *Reticulofenestrid* coccoliths from the Southern Ocean sites (e.g. ODP 1090) were two times as large as those in the tropical Atlantic (ODP 925, 929) during the Eocene–Oligocene transition. This apparent cell size variability of alkenone producers hampers the application of available coccolith data to the $HCO_3^- - CO_2$ conversion evaluation of the Cenozoic. Therefore, given that cell size data for the past 40 million years are not available for Site 925, we assume a constant cell radius of 2.67 µm, which is the average value estimated from coccolith dimensions for the Cenozoic [21,37,89].

Boron isotope-derived seawater pH and coeval Mg/Ca-based SST, with the assumption of a constant salinity of 35 and 2.67 µm cell radius of alkenone producers, enables an assessment of the impact of bicarbonate–CO_2 conversion on alkenone–pCO_2 estimates during the Cenozoic. Temporal patterns in the ratio r/r_k indicate that the percentage of fixed carbon derived from bicarbonate conversion is generally low, of the order of 1.4–2.3% (figure 6), with a trend of elevated bicarbonate contribution by the Pleistocene (approx. 40% more relative to the Late Eocene; figure 6). Since we assume constant cell size, this increase is primarily due to an approximately 0.5 pH drop from approximately 7.7 during the latest Eocene [16] to 8.2 today. Alternatively, CCMs could have become increasingly important [50,96] to counter low CO_2. However, accurate quantitative correction for the effect of $HCO_3^- - CO_2$ conversion on alkenone–pCO_2 estimates will require more detailed site-specific data on cell size of the alkenone producers and pH history of the region.

An alternative model to estimate CCM activity [44,50] considers both diffusion and active uptake of inorganic carbon to describe the nonlinear culture results of *P. tricornutum*:

$$\varepsilon_p = \varepsilon_f + \varepsilon_t - \varepsilon_{-t} - \left(\frac{1}{1 + C_e P/\mu C(1+\beta)}\right)\left(\frac{\varepsilon_f - \varepsilon_{-t}}{\beta + 1}\right). \tag{5.6}$$

Here, β is a constant equivalent to the ratio of CO_2 loss (leakage by diffusion) to carbon fixation, P is membrane permeability, C is cell carbon content and ε_{-t} is the isotopic fractionation

associated with the inorganic carbon diffusion back from the cell to the surrounding seawater. As detailed in Laws *et al*. [50], the value of ε_p becomes insensitive to $\mu/[CO_{2(aq)}]$ when

$$\frac{\mu}{C_e} \geq \frac{P}{C(1+\beta)}. \tag{5.7}$$

Empirical relationships between P and C show its dependence on the cell radius: $P/C = 0.285\, r^{-1}$. Minimum $[CO_{2(aq)}]$ that would trigger active transport occurs when the term $(1+\beta)$ approaches unity, or leakage is zero. Laws *et al*. [50] calculate that ε_p for *E. huxleyi* would become a nonlinear function of $\mu/[CO_{2(aq)}]$ as photoperiod growth rate exceeds $1.1\,d^{-1}$ for a cell radius of $2.6\,\mu m$, comparable with the culture results of *E. huxleyi* [42].

Growth rates in the natural environment for *E. huxleyi* and other alkenone-producing haptophytes are generally low, below $1\,d^{-1}$, ranging from 0.1 to $1\,d^{-1}$ [53,97]. Cell dimensions of alkenone-producing algae since Middle Eocene [18,21,37,89] used in conjunction with estimates of pCO_2 provide a means to identify geologic intervals when upregulation of CCMs was potentially necessary. For example, cell radii for alkenone producers range from approximately 4 to $2.4\,\mu m$ during the Eocene–Oligocene transition [21], and cell radii were about 50% smaller during the Early Miocene [37]. Knowledge of cell radius allows calculation of the ratio P/C [50] and the ratio $\mu/[CO_{2(aq)}]$ can be estimated from alkenone-based CO_2 reconstructions and a range of modern haptophyte growth rates, assuming alkenone-based CO_2 estimates are valid even if CCMs were active. Using pCO_2 data from earlier results [19,20,28], figure 6 shows that for low to moderate growth rates, the operation of CCMs is expected during the Miocene, particularly during the climatic optimum of the late Early Miocene, suggesting that the alkenone–CO_2 estimates may be compromised during this time interval. Obviously, this result is speculative given the necessary assumptions. For example, CO_2 concentrations used in this exercise derive from alkenone measurements and if CCMs were active, then these CO_2 values would appear artificially lower than actual concentrations and further exaggerate the potential influence of CCMs.

6. Conclusions

An alkenone-based pCO_2 record spanning the past 40 million years is presented for ODP Site 925—representing the first long-term Cenozoic pCO_2 record constructed from a single site. Facilitated by improved methodology and careful consideration of assumptions, this record provides refined pCO_2 estimates from a site that is characterized by limited long-term variability in oceanographic conditions. This record, therefore, reflects our most up-to-date effort to better constrain the Cenozoic history of atmospheric CO_2. This new record confirms predictions from climate models regarding the role of CO_2 in the cryosphere evolution in both hemispheres at several key time intervals (e.g. Eocene–Oligocene transition, MMCT, Plio-Pleistocene). This record also suggests that Miocene CO_2 levels were higher than earlier estimates, which better reconciles a long-standing data–model discrepancy for the Miocene. However, outstanding issues remain which include the presumed warming or deglaciation in the Late Oligocene and the abrupt and transient oxygen isotope excursion at Mi-1, both of which challenge our understanding of CO_2 climate and ice sheet sensitivity.

We also evaluate spontaneous $HCO_3^- - CO_{2(aq)}$ conversion, which is one variable that could impact CO_2 estimates from the alkenone–pCO_2 method. We conclude that the contribution from $HCO_3^- - CO_2$ conversion to the carbon fixed by alkenone-producing algae is minor, although this potential has increased by 40% from Late Eocene to the Quaternary. Finally, an exercise to evaluate potential CCM activity in haptophyte algae suggests that low pCO_2 levels in the Neogene are more likely to trigger CCMs.

Acknowledgements. We thank Dan Lunt for his editorial handling, Rich Pancost and an anonymous reviewer for their thoughtful reviews.

Funding statement. This study was supported by NSF AGS P2C2 award 1203163 to M.P. and R.D.

References

1. Keeling CD. 1960 The concentration and isotopic abundances of carbon dioxide in the atmosphere. *Tellus* **12**, 200–203. (doi:10.1111/j.2153-3490.1960.tb01300.x)
2. Petit JR *et al*. 1999 Climate and atmospheric history of the past 420,000 years from the Vostok ice core, Antarctica. *Nature* **399**, 429–436. (doi:10.1038/20859)
3. Luthi D *et al*. 2008 High-resolution carbon dioxide concentration record 650,000–800,000 years before present. *Nature* **453**, 379–382. (doi:10.1038/nature06949)
4. Siegenthaler U *et al*. 2005 Stable carbon cycle–climate relationship during the Late Pleistocene. *Science* **310**, 1313–1317. (doi:10.1126/science.1120130)
5. van der Burgh J, Visscher H, Dilcher DL, Kurschner WM. 1993 Paleoatmospheric signatures in Neogene fossil leaves. *Science* **260**, 1788–1790. (doi:10.1126/science.260.5115.1788)
6. Kurschner WM, Kvacek Z, Dilcher DL. 2008 The impact of Miocene atmospheric carbon dioxide fluctuations on climate and evolution of terrestrial ecosystems. *Proc. Natl Acad. Sci. USA* **105**, 449–453. (doi:10.1073/pnas.0708588105)
7. Kurschner WM. 1996 Leaf stomata as biosensors of paleoatmospheric CO_2 levels. *LPP Contrib. Ser.* **5**, 1–153.
8. Royer DL. 2001 Stomatal density and stomatal index as indicators of paleoatmospheric CO_2 concentration. *Rev. Palaeobot. Palynol.* **114**, 1–28. (doi:10.1016/s0034-6667(00)00074-9)
9. Retallack GJ. 2009 Greenhouse crises of the past 300 million years. *GSA Bull.* **121**, 1441–1455. (doi:10.1130/B26341.1)
10. Ekart DD, Cerling TE, Montanez IP, Tobor A. 1999 400 million year carbon isotope record of pedogenic carbonates: implications for paleoatmospheric carbon dioxide. *Am. J. Sci.* **299**, 805–827. (doi:10.2475/ajs.299.10.805)
11. Retallack GJ. 2009 Refining a pedogenic-carbonate CO_2 paleobarometer to quantify a Middle Miocene greenhouse spike. *Palaeogeogr. Palaeoclimatol. Palaeoecol.* **281**, 57–65. (doi:10.1016/j.palaeo.2009.07.011)
12. Cerling TE. 1992 Use of carbon isotopes in paleosols as an indicator of the $p(CO_2)$ of the paleoatmosphere. *Global Biogeochem. Cyc.* **6**, 307–314. (doi:10.1029/92GB01102)
13. Honisch B, Hemming GN, Archer D, Siddall M, McManus JF. 2009 Atmospheric carbon dioxide concentration across the Mid-Pleistocene transition. *Science* **324**, 1551–1554. (doi:10.1126/science.1171477)
14. Bartoli G, Honisch B, Zeebe RE. 2011 Atmospheric CO_2 decline during the Pliocene intensification of Northern Hemisphere glaciation. *Paleoceanography* **26**, PA4213. (doi:10.1029/2010PA002055)
15. Foster GL, Lear CH, Rae JWB. 2012 The evolution of pCO_2, ice volume and climate during the Middle Miocene. *Earth Planet. Sci. Lett.* **341–344**, 243–254. (doi:10.1016/j.epsl.2012.06.007)
16. Pearson PN, Foster GL, Wade BS. 2009 Atmospheric carbon dioxide through the Eocene–Oligocene climate transition. *Nature* **461**, 1110–1113. (doi:10.1038/nature08447)
17. Sanyal A, Hemming NG, Hanson GN, Broecker WS. 1995 Evidence for a higher pH in the glacial ocean from boron isotopes in foraminifera. *Nature* **373**, 234–236. (doi:10.1038/373234a0)
18. Seki O, Foster GL, Schmidt DN, Mackensen A, Kawamura K, Pancost RD. 2010 Alkenone and boron-based Pliocene pCO_2 records. *Earth Planet. Sci. Lett.* **292**, 201–211. (doi:10.1016/j.epsl.2010.01.037)
19. Pagani M, Authur MA, Freeman KH. 1999 Miocene evolution of atmospheric carbon dioxide. *Paleoceanography* **14**, 273–292. (doi:10.1029/1999PA900006)
20. Pagani M, Freeman KH, Arthur MA. 1999 Late Miocene atmospheric CO_2 concentrations and the expansion of C_4 grasses. *Science* **285**, 876–879. (doi:10.1126/science.285.5429.876)
21. Pagani M, Huber M, Liu ZH, Bohaty S, Henderiks J, Sijp W, Krishnan S, DeConto R. 2011 The role of carbon dioxide during the onset of Antarctic glaciation. *Science* **334**, 1261–1264. (doi:10.1126/science.1203909)
22. Pagani M, Liu ZH, LaRiviere J, Ravelo AC. 2010 High Earth-system climate sensitivity determined from Pliocene carbon dioxide concentrations. *Nat. Geosci.* **3**, 27–30. (doi:10.1038/ngeo724)
23. Bijl PK, Houben AJP, Schouten S, Bohaty S, Sluijs A, Reichart GJ, Damste JSS, Brinkhuis H. 2010 Transient Middle Eocene atmospheric CO_2 and temperature variations. *Science* **330**, 819–821. (doi:10.1126/science.1193654)

24. Palmer MR, Brummer GJ, Cooper MJ, Elderfield H, Greaves MJ, Reichart GJ, Schouten S, Yu JM. 2010 Multi-proxy reconstruction of surface water pCO_2 in the northern Arabian Sea since 29 ka. *Earth Planet. Sci. Lett.* **295**, 49–57. (doi:10.1016/j.epsl.2010.03.023)
25. Beerling DJ, Royer DL. 2011 Convergent Cenozoic CO_2 history. *Nat. Geosci.* **4**, 418–420. (doi:10.1038/ngeo1186)
26. Jasper JP, Hayes JM. 1990 A carbon isotope record of CO_2 levels during the Late Quaternary. *Nature* **347**, 462–464. (doi:10.1038/347462a0)
27. Jasper JP, Hayes JM, Mix AC, Prahl FG. 1994 Photosynthetic fractionation of ^{13}C and concentrations of dissolved CO_2 in the central equatorial Pacific during the last 255,000 years. *Paleoceanography* **9**, 781–798. (doi:10.1029/94PA02116)
28. Pagani M, Zachos JC, Freeman KH, Tipple B, Bohaty S. 2005 Marked decline in atmospheric carbon dioxide concentrations during the Paleogene. *Science* **309**, 600–603. (doi:10.1126/science.1110063)
29. Conte M, Volkman JK, Eglinton G. 1994 Lipid biomarkers of the Haptophyta. In *The haptophyte algae* (eds JC Green, BSC Leadbeater), pp. 351–377. Oxford, UK: Clarendon Press.
30. Volkman JK, Barrett SM, Blackburn SI, Sikes EL. 1995 Alkenones in *Gephyrocapsa oceanica*: implications for studies of paleoclimate. *Geochim. Cosmochim. Acta* **59**, 513–520. (doi:10.1016/0016-7037(95)00325-T)
31. McIntyre A. 1970 *Gephyrocapsa protohyxleyi* sp. n. a possible phyletic link and index fossil for the Pleistocene. *Deep Sea Res. I* **17**, 187–190. (doi:10.1016/0011-7471(70)90097-5)
32. Hay WW. 1977 Calcareous nannofossils. In *Oceanic micropaleontology* (ed. ATS Ramsey), pp. 1–48. London, UK: Academic Press.
33. Young J. 1990 Size variation of Neogene *Reticulofenestra* coccoliths from Indian Ocean DSDP cores. *J. Micropalaeontol.* **9**, 71–85. (doi:10.1144/jm.9.1.71)
34. Marlowe IT, Brassell SC, Eglinton G, Green JC. 1990 Long-chain alkenones and alkyl alkenoates and the fossil coccolith record of marine sediments. *Chem. Geol.* **88**, 349–375. (doi:10.1016/0009-2541(90)90098-R)
35. Young JR. 1998 Neogene. In *Calcareous nannofossil biostratigraphy* (ed. PR Bown), pp. 225–265. New York, NY: Springer.
36. Plancq J, Grossi V, Henderiks J, Simon L, Mattioli E. 2012 Alkenone producers during Late Oligocene–Early Miocene revisited. *Paleoceanography* **27**, PA1202. (doi:10.1029/2011PA002164)
37. Henderiks J, Pagani M. 2007 Refining ancient carbon dioxide estimates: significance of coccolithophore cell size for alkenone-based pCO_2 records. *Paleoceanography* **22**, PA3202. (doi:10.1029/2006PA001399)
38. Popp BN, Kenig F, Wakeham SG, Laws EA, Bidigare RR. 1998 Does growth rate affect ketone unsaturation and intracellular carbon isotopic variability in *Emiliania hyxleyi? Paleoceanography* **13**, 35–41. (doi:10.1029/97PA02594)
39. Farquhar GD, Ehleringer JR, Hubick KT. 1989 Carbon isotope discrimination and photosynthesis. *Annu. Rev. Plant Physiol. Plant Mol. Biol.* **40**, 503–537. (doi:10.1146/annurev.pp.40.060189.002443)
40. Farquhar GD, O'Leary MH, Berry JA. 1982 On the relationship between carbon isotope discrimination and the intercellular carbon dioxide concentration in leaves. *Aust. J. Plant Physiol.* **9**, 121–137. (doi:10.1071/PP9820121)
41. Goericke R, Montoya JP, Fry B. 1994 Physiology of isotope fractionation in algae and cyanobateria. In *Stable isotope in ecology* (eds K Lajtha, B Michener), pp. 187–221. Cambridge, UK: Blackwell Scientific.
42. Popp BN, Laws EA, Bidigare RR, Dore JE, Hanson KL, Wakeham SG. 1998 Effect of phytoplankton cell geometry on carbon isotopic fractionation. *Geochim. Cosmochim. Acta* **62**, 69–77. (doi:10.1016/s0016-7037(97)00333-5)
43. Laws EA, Popp BN, Bidigare RR, Kennicutt MC, Macko SA. 1995 Dependence of phytoplankton carbon isotopic composition on growth rate and $[CO_2]_{aq}$: theoretical considerations and experimental results. *Geochim. Cosmochim. Acta* **59**, 1131–1138. (doi:10.1016/0016-7037(95)00030-4)
44. Laws EA, Bidigare RR, Popp BN. 1997 Effect of growth rate and CO_2 concentration on carbon isotopic fractionation by the marine diatom *Phaeodactylum tricornutum*. *Limnol. Oceanogr.* **42**, 1552–1560. (doi:10.4319/lo.1997.42.7.1552)
45. Riebesell U, Revill AT, Holdsworth DG, Volkman JK. 2000 The effects of varying CO_2 concentration on lipid composition and carbon isotope fractionation in *Emiliania huxleyi*. *Geochim. Cosmochim. Acta* **64**, 4179–4192. (doi:10.1016/s0016-7037(00)00474-9)

46. Rost B, Zondervan I, Riebesell U. 2002 Light-dependent carbon isotope fractionation in the coccolithophorid *Emiliania huxleyi*. *Limnol. Oceanogr.* **47**, 120–128. (doi:10.4319/lo.2002.47.1.0120)
47. Burkhardt S, Riebesell U, Zondervan I. 1999 Effects of growth rate, CO_2 concentration, and cell size on the stable carbon isotope fractionation in marine phytoplankton. *Geochim. Cosmochim. Acta* **63**, 3729–3741. (doi:10.1016/s0016-7037(99)00217-3)
48. Raven JA, Johnston AM. 1991 Mechanisms of inorganic-carbon acquisition in marine phytoplankton and their implications for the use of other resources. *Limnol. Oceanogr.* **36**, 1701–1714. (doi:10.4319/lo.1991.36.8.1701)
49. Raven JA, Johnston AM, Turpin DH. 1993 Influence of changes in CO_2 concentration and temperature on marine phytoplankton $^{13}C/^{12}C$ ratios: an analysis of possible mechanisms. *Global Planet. Change* **8**, 1–12. (doi:10.1016/0921-8181(93)90058-v)
50. Laws EA, Popp BN, Cassar N, Tanimoto J. 2002 ^{13}C discrimination patterns in oceanic phytoplankton: likely influence of CO_2 concentrating mechanisms, and implications for palaeoreconstructions. *Funct. Plant Biol.* **29**, 323–333. (doi:10.1071/PP01183)
51. Giordano M, Beardall J, Raven JA. 2005 CO_2 concentrating mechanisms in algae: mechanisms, environmental modulation, and evolution. *Annu. Rev. Plant Biol.* **56**, 99–131. (doi:10.1146/annurev.arplant.56.032604.144052)
52. Rau GH, Riebesell U, Wolf-Gladrow D. 1996 A model of photosynthetic ^{13}C fractionation by marine phytoplankton based on diffusive molecular CO_2 uptake. *Mar. Ecol. Prog. Ser.* **133**, 275–285. (doi:10.3354/meps133275)
53. Bidigare RR *et al*. 1997 Consistent fractionation of ^{13}C in nature and in the laboratory: growth-rate effects in some haptophyte algae. *Glob. Biogeochem. Cyc.* **11**, 279–292. (doi:10.1029/96GB03939)
54. Hay WW *et al.* 1999 An alternative global Cretaceous paleogeography. In *The evolution of Cretaceous ocean/climate systems* (eds E Barrera, C Johnson), pp. 1–48. Boulder, CO: Geological Society of America.
55. Shipboard Scientific Party. 1995 Site 925. In *Proc. Ocean Drilling Program, initial reports* (eds WB Curry, NJ Shackleton, C Richter), pp. 55–152. College Station, TX: Ocean Drilling Program.
56. Conkright ME, Locarnini RA, Garcia HE, O'Brien TD, Boyer TP, Stephens C, Antonov JI. 2002 *World ocean atlas 2001: objective analyses, data statistics, and figures*. Silver Springs, MD: National Oceanographic Data Center.
57. Nilsen EB, Anderson LD, Delaney ML. 2003 Paleoproductivity, nutrient burial, climate change and the carbon cycle in the western equatorial Atlantic across the Eocene/Oligocene boundary. *Paleoceanography* **18**, 1057. (doi:10.1029/2002PA000804)
58. Takahashi T *et al*. 2009 Climatological mean and decadal change in surface ocean pCO_2, and net sea–air CO_2 flux over the global oceans. *Deap-Sea Res. II* **56**, 554–577. (doi:10.1016/j.dsr2.2008.12.009)
59. Prahl FG, Wakeham SG. 1987 Calibration of unsaturation patterns in long-chain ketone compositions for palaeotemperature assessment. *Nature* **330**, 367–369. (doi:10.1038/330367a0)
60. Brassell SC, Eglinton G, Marlowe IT, Pflaumann U, Sarnthein M. 1986 Molecular stratigraphy: a new tool for climatic assessment. *Nature* **320**, 129–133. (doi:10.1038/320129a0)
61. Hopmans EC, Schouten S, Pancost RD, van der Meer MTJ, Sinnighe Damste JS. 2000 Analysis of intact tetraether lipids in archaeal cell material and sediments by high performance liquid chromatography/atmospheric pressure chemical ionization mass spectrometry. *Rapid Commun. Mass Spectrom.* **14**, 585–589. (doi:10.1002/(SICI)1097-0231(20000415)14:7<585::AID-RCM913>3.0.CO;2-N)
62. Schouten S, Hopmans EC, Schefuss E, Damste JSS. 2002 Distributional variations in marine crenarchaeotal membrane lipids: a new tool for reconstructing ancient sea water temperatures? *Earth Planet. Sci. Lett.* **204**, 265–274. (doi:10.1016/S0012-821X(02)00979-2)
63. Pearson PN, Chaisson WP. 1997 Late Paleocene to Middle Miocene planktonic foraminifer biostratigraphy of the Ceara Rise. In *Proc. Ocean Drilling Program, scientific results* (eds NJ Shackleton, WB Curry, RA Richards, TJ Bralower), pp. 33–68. College Station, TX: Ocean Drilling Program.
64. Chaisson WP, Pearson PN. 1997 Planktonic foraminifer biostratigraphy at Site 925: Middle Miocene–Pleistocene. In *Proc. Ocean Drilling Program, scientific results* (eds NJ Shackleton, WB Curry, C Richter, TJ Bralower), pp. 3–31. College Station, TX: Ocean Drilling Program.
65. Cande SC, Kent DV. 1995 Revised calibration of the geomagnetic polarity timescale for the Late Cretaceous and Cenozoic. *J. Geophys. Res.* **100**, 6093–6095. (doi:10.1029/94JB03098)

66. Berggren WA, Kent DV, Swisher CC, Aubry M-P. 1995 A revised Cenozoic geochronology and chronostratigraphy. In *Geochronology, time scales and global stratigraphic correlation* (eds WA Berggren, DV Kent, M-P Aubry, J Hardenbol), pp. 129–212. Tulsa, OK: SEPM Society for Sedimentary Geology.
67. Conte M, Sicre M-A, Ruhlemann C. 2006 Global temperature calibration of the alkenone unsaturation index ($U^{K'}_{37}$) in surface waters and comparison with surface sediments. *Geochem. Geophys. Geosyst.* **7**, Q02005. (doi:10.1029/2005GC001054)
68. Liu Z, Pagani M, Zinniker D, DeConto R, Huber M, Brinkhuis H, Shah SR, Leckie RM, Pearson A. 2009 Global cooling during the Eocene-Oligocene climate transition. *Science* **323**, 1187–1190. (doi:10.1126/science.1166368)
69. Hopmans EC, Weijers JWH, Schefuß E, Herfort L, Sinninghe Damsté JS, Schouten S. 2004 A novel proxy for terrestrial organic matter in sediments based on branched and isoprenoid tetraether lipids. *Earth Planet. Sci. Lett.* **224**, 107–116. (doi:10.1016/j.epsl.2004.05.012)
70. Spero HJ, Mielke KM, Kalve EM, Lea DW, Pak DK. 2003 Multispecies approach to reconstructing eastern equatorial Pacific thermocline hydrography during the past 360 kyr. *Paleoceanography* **18**, 1022. (doi:10.1029/2002PA000814)
71. DeConto RM, Pollard D, Wilson PA, Palike H, Lear CH, Pagani M. 2008 Thresholds for Cenozoic bipolar glaciation. *Nature* **455**, 652–656. (doi:10.1038/nature07337)
72. Zachos JC, Dickens GR, Zeebe RE. 2008 An Early Cenozoic perspective on greenhouse warming and carbon-cycle dynamics. *Nature* **451**, 279–283. (doi:10.1038/nature06588)
73. DeConto R, Pollard D. 2003 Rapid Cenozoic glaciation of Antarctica induced by declining atmospheric CO_2. *Nature* **421**, 245–249. (doi:10.1038/nature01290)
74. Knauss JA. 2006 *Introduction to physical oceanography*, p. 309, 2nd edn. Long Grove, IL: Waveland Press.
75. Palike H, Norris RD, Herrle JO, Wilson PA, Coxall HK, Lear CH, Shackleton NJ, Tripati A, Wade BS. 2006 The heartbeat of the Oligocene climate system. *Science* **314**, 1894–1898. (doi:10.1126/science.1133822)
76. Miller KG, Wright JD, Fairbanks RG. 1991 Unlocking the ice house: Oligocene to Miocene oxygen isotopes eustasy and margin erosion. *J. Geophys. Res.* **96**, 6829–6848. (doi:10.1029/90JB02015)
77. Lear CH, Rosenthal Y, Coxall HK, Wilson PA. 2004 Late Eocene to Early Miocene ice sheet dynamics and the global carbon cycle. *Paleoceanography* **19**, PA4015. (doi:10.1029/2004PA001039)
78. Pollard D, DeConto RM. 2005 Hysteresis in Cenozoic Antarctic ice-sheet variations. *Glob. Planet. Change* **45**, 9–21. (doi:10.1016/j.gloplacha.2004.09.011)
79. Hague AM, Thomas DJ, Huber M, Korty R, Woodard SC, Jones LB. 2012 Convection of North Pacific deep water during the Early Cenozoic. *Geology* **40**, 527–530. (doi:10.1130/G32886.1)
80. Thomas DJ, Lyle M, Moore Jr TC, Rea DK. 2008 Paleogene deepwater mass composition of the tropical Pacific and implications for thermohaline circulation in a greenhouse world. *Geochem. Geophys. Geosyst.* **9**, Q02002. (doi:10.1029/2007GC001748)
81. Pearson PN, Palmer MR. 2000 Atmospheric carbon dioxide concentrations over the past 60 million years. *Nature* **406**, 695–699. (doi:10.1038/35021000)
82. Lunt DJ, Foster GL, Haywood AM, Stone EJ. 2008 Late Pliocene Greenland glaciation controlled by a decline in atmospheric CO_2 levels. *Nature* **454**, 1102–1105. (doi:10.1038/nature07223)
83. Ruddiman WF. 2010 A paleoclimatic enigma? *Science* **328**, 838–839. (doi:10.1126/science.1188292)
84. LaRiviere JP, Ravelo AC, Crimmins A, Dekens PS, Ford HL, Lyle M, Wara MW. 2012 Late Miocene decoupling of oceanic warmth and atmospheric carbon dioxide forcing. *Nature* **486**, 97–100. (doi:10.1038/nature11200)
85. You Y, Huber M, Muller RD, Poulsen CJ, Ribbe J. 2009 Simulation of the Middle Miocene climate optimum. *Geophys. Res. Lett.* **36**, L04702. (doi:10.1029/2008GL036571)
86. Holbourn A, Kuhnt W, Schulz M, Erlenkeuser H. 2005 Impacts of orbital forcing and atmospheric carbon dioxide on Miocene ice-sheet expansion. *Nature* **438**, 483–487. (doi:10.1038/nature04123)
87. Badger MR, Andrews TJ, Whitney SM, Ludwig M, Yellowlees DC, Leggat W, Price GD. 1998 The diversity and coevolution of Rubisco, plastids, pyrenoids, and chloroplast-based CO_2-concentrating mechanisms in algae. *Can. J. Bot.* **76**, 1052–1071. (doi:10.1139/cjb-76-6-1052)

88. Rickaby REM, Henderiks J, Young JN. 2010 Perturbing phytoplankton: response and isotopic fractionation with changing carbonate chemistry in two coccolithophore species. *Clim. Past* **6**, 771–785. (doi:10.5194/cp-6-771-2010)
89. Henderiks J, Pagani M. 2008 Coccolithophore cell size and the Paleogene decline in atmospheric CO_2. *Earth Planet. Sci. Lett.* **269**, 575–583. (doi:10.1016/j.epsl.2008.03.016)
90. Riebesell U, Wolf-Gladrow DA, Smetacek V. 1993 Carbon dioxide limitation of marine phytoplankton growth rates. *Nature* **361**, 249–251. (doi:10.1038/361249a0)
91. Wolf-Gladrow D, Riebesell U. 1997 Diffusion and reactions in the vicinity of plankton: a refined model for inorganic carbon transport. *Mar. Chem.* **59**, 17–34. (doi:10.1016/S0304-4203(97)00069-8)
92. Kameo KT, Bralower TJ. 2000 Size variation of reticulofenestra coccoliths during the Neogene. In *Proc. Ocean Drilling Program—scientific results* (eds RM Leckie, J Sigurdsson), pp. 3–17. College Station, TX: Ocean Drilling Program.
93. Jahne B, Heinz G, Dietrich W. 1987 Measurement of the diffusion coefficients of sparingly soluble gases in water. *J. Geophys. Res.* **92**, 10 767–10 776. (doi:10.1029/JC092iC10p10767)
94. Gavis J, Ferguson JF. 1975 Kinetics of carbon dioxide uptake by phytoplankton at high pH. *Limnol. Oceanogr.* **20**, 211–221. (doi:10.4319/lo.1975.20.2.0211)
95. US DOE. 1994 *Handbook of methods for the analysis of the various parameters of the carbon dioxide system in sea water*, ORNL-CDIAC-74 (eds AG Dickson, C Goyet). Washington, DC: US Department of Energy.
96. Pagani M. In press. Biomarker-based inferences of past climate: the alkenone pCO_2 proxy. In *Treatise on geochemistry* (eds HD Holland, KK Turekian). Amsterdam, The Netherlands: Elsevier.
97. Popp BN, Bidigare RR, Deschenes B, Laws EA, Prahl FG, Tanimoto J, Wallsgrove RJ. 2006 A new method for estimating growth rates of alkeone-producing haptophytes. *Limnol. Oceanogr. Methods* **4**, 114–129. (doi:10.4319/lom.2006.4.114)